

Metformin Abrogates Age-Associated Ovarian Fibrosis

Curtis W. McCloskey^{1,2}, David P. Cook^{1,2}, Brendan S. Kelly^{1,2}, Feryel Azzi^{3,4}, Christian H. Allen⁵, Amanda Forsyth⁶, Jeremy Upham⁷, Katey J. Rayner⁸, Douglas A. Gray¹, Robert W. Boyd⁷, Sangeeta Murugkar⁵, Bryan Lo^{1,9,10}, Dominique Trudel^{3,4}, Mary K. Senterman^{6,10}, and Barbara C. Vanderhyden^{1,2}



ABSTRACT

Purpose: The ovarian cancer risk factors of age and ovulation are curious because ovarian cancer incidence increases in postmenopausal women, long after ovulations have ceased. To determine how age and ovulation underlie ovarian cancer risk, we assessed the effects of these risk factors on the ovarian microenvironment.

Experimental Design: Aged C57/lcrfa mice (0–33 months old) were generated to assess the aged ovarian microenvironment. To expand our findings into human aging, we assembled a cohort of normal human ovaries ($n = 18$, 21–71 years old). To validate our findings, an independent cohort of normal human ovaries was assembled ($n = 9$, 41–82 years old).

Results: We first validated the presence of age-associated murine ovarian fibrosis. Using interdisciplinary methodologies,

we provide novel evidence that ovarian fibrosis also develops in human postmenopausal ovaries across two independent cohorts ($n = 27$). Fibrotic ovaries have an increased CD206⁺:CD68⁺ cell ratio, CD8⁺ T-cell infiltration, and profibrotic DPP4⁺αSMA⁺ fibroblasts. Metformin use was associated with attenuated CD8⁺ T-cell infiltration and reduced CD206⁺:CD68⁺ cell ratio.

Conclusions: These data support a novel hypothesis that unifies the primary nonhereditary ovarian cancer risk factors through the development of ovarian fibrosis and the formation of a premetastatic niche, and suggests a potential use for metformin in ovarian cancer prophylaxis.

See related commentary by Madariaga et al., p. 523

Introduction

Ovarian cancers are the fifth leading cause of cancer-associated death in women and the most lethal among gynecologic malignancies (1). Five-year survival is estimated at 47.4% in part due to a lack of sensitive screening methods to detect early disease and a lack of treatments for chemotherapy-refractive patients (2). Given the difficulty in detecting and treating ovarian cancer, the development of novel prevention methods is a sought-after public health goal.

Current methods for risk reduction are restricted to surgical salpingo-oophorectomy and use of oral contraceptives, both of which have limitations. In seeking novel ovarian cancer prevention strategies,

studying established risk factors can offer new insights. Age and the number of lifetime ovulations are the primary nonhereditary risk factors and are proportional to risk (1, 3, 4), and *BRCA* mutations are the primary hereditary risk factors with differential risk conferred by the site of mutation (5). Curiously, the median age at diagnosis of ovarian cancer is 63 years old, years after ovulations have normally ceased at menopause (2). Taken together, this led us to explore if age and ovulations could transform the ovarian microenvironment into a niche that is permissive to ovarian cancer growth.

Ovulation requires extensive architectural remodeling of the extracellular matrix (ECM) that may alter the ovarian microenvironment over time. Interestingly, age-associated stromal fibrosis was recently shown to occur in aged mice (6). This fibrosis correlated with a proinflammatory cascade with increased F4/80⁺ macrophage infiltration and proinflammatory chemokines postulated to reduce gamete quality with age (6). Over a century ago, Paget established the “seed and soil” hypothesis upon the observation that some tissues are more prone to cancer metastasis (7). Fibrosis has since been established as a fertile “soil” or premetastatic niche for cancer metastasis in models of cancer cell colonization of fibrotic lungs, and in fibrotic breast disease (8, 9).

Fibrotic niches provide mechanosensory signals and have a characteristic chronic inflammatory response that provides a cytokine milieu that can consequently aid metastatic invasion and colonization (10–12). The age-associated murine ovarian fibrosis reported by Briley and colleagues has yet to be extended to human aging, but the human ovary is an established protumor niche. Many cancers discovered in the ovary are metastases from other primary malignancies, commonly from fallopian tube, breast, colon, or gastric origin (13–15). However, the reason these metastases are attached to the ovary remains unknown.

Metformin has been demonstrated to treat and prevent fibrosis in preclinical models of lung, kidney, liver, skin, and heart fibrosis through the AMPK-mediated suppression of TGFβ production (16–20). Interestingly, in a robust retrospective analysis of women with type II diabetes (T2D) using metformin compared with nonusers,

¹Cancer Therapeutics Program, Ottawa Hospital Research Institute, 501 Smyth Road, Ottawa, Ontario, Canada. ²Department of Cellular and Molecular Medicine, University of Ottawa, Ottawa, Ontario, Canada. ³Institut du Cancer de Montréal and Centre de recherche du Centre hospitalier de l'Université de Montréal, Montréal, Quebec, Canada. ⁴Department of Pathology and Cellular Biology, Université de Montréal, Montréal, Quebec, Canada. ⁵Department of Physics, Carleton University, Ottawa, Ontario, Canada. ⁶Department of Obstetrics and Gynecology, University of Ottawa, Ottawa, Ontario, Canada. ⁷Department of Physics and School of Electrical Engineering and Computer Science, University of Ottawa, Ottawa, Canada. ⁸University of Ottawa Heart Institute, Department of Biochemistry, Microbiology and Immunology, Faculty of Medicine, Ottawa, Ontario, Canada. ⁹Molecular Oncology Diagnostics Laboratory, Division of Anatomical Pathology, The Ottawa Hospital, Ottawa, Ontario, Canada. ¹⁰Department of Pathology and Laboratory Medicine, University of Ottawa, Ottawa, Ontario, Canada.

Note: Supplementary data for this article are available at Clinical Cancer Research Online (<http://clincancerres.aacrjournals.org/>).

Corresponding Author: Barbara C. Vanderhyden, Ottawa Hospital Research Institute, 501 Smyth Road, 3rd Floor, Box 926, Ottawa, Ontario K1H 8L6, Canada. Phone: 613-737-7700; Fax: 613-247-3524; E-mail: bvanderhyden@ohri.ca

Clin Cancer Res 2020;26:632–42

doi: 10.1158/1078-0432.CCR-19-0603

©2019 American Association for Cancer Research.

Translational Relevance

This study provides novel evidence that ovarian fibrosis develops with age in women. Ovarian fibrosis was found to correlate with immune and stromal features that are characteristic of a tumor-permissive niche. The development of this tumor-permissive niche with age offers a novel explanation for the long-standing conundrum that ovulation is a primary nonhereditary risk factor for ovarian cancer, yet the median age of ovarian cancer diagnosis is 63 years old, years after ovulations have ceased at menopause. It also helps to explain why the ovary is a common metastatic site for cancer from other organs, including the fallopian tube. Interestingly, metformin use by postmenopausal women was sufficient to abrogate both ovarian fibrosis and features of a tumor-permissive niche, providing translational support and setting the stage for large-scale studies to investigate the efficacy of metformin use for ovarian cancer prevention.

metformin users had up to an astonishing 88% reduction in ovarian cancer incidence (21). This risk-reducing effect of metformin on ovarian cancer incidence has recently been confirmed in a meta-analysis (22). This led us to hypothesize that metformin use prevents age-associated ovarian fibrosis, thereby preventing the development of a tumor-permissive niche and decreasing the risk of ovarian cancer. In this study, we first validate the presence of age-associated fibrosis in murine ovaries and then extend these findings to two independent cohorts of premenopausal and postmenopausal human ovaries with or without metformin use, providing support for a novel hypothesis underlying the age-associated risk of ovarian cancer.

Materials and Methods

Patient samples

Ovarian samples were acquired from oophorectomies performed at The Ottawa Hospital and at the Centre hospitalier de l'Université de Montréal (CHUM, Montréal, Quebec, Canada). Samples were retrieved from archived tissues with protocol approval of the Ottawa Health Science Network Research Ethics Board. All samples were deemed normal and noncancerous. Menopausal status was determined using age, histology, and medical records by experienced pathologists (M.K. Senterman and D. Trudel). Specifically, a lack of menses for at least 12 months, age >54, and a lack of both primordial follicles and recent follicular activity (such as regressing corpus lutea) were used to define postmenopausal ovaries. In addition, no postmenopausal case had used hormone replacement therapy. It has been reported that different ovarian cancer subtypes vary in unilateral versus bilateral presentation (23), and there is evidence that contralateral ovaries may age differently because ovulation tends to occur proportionately between contralateral ovaries in younger women, but becomes much less proportionate with age (24). We therefore included contralateral ovarian samples as separate replicates. Exclusion criteria was set based on the reasoning for ovary removal, *BRCA* mutation status, family history, prescription drug usage, and histology. Patients with contralateral ovarian malignancy were excluded. Patients were also excluded if taking testosterone or Lupron. Samples from The Ottawa Hospital were processed as follows: Large regions of ovarian cortex (often bilateral samples represented by numerous samples per case in **Table 1**) were isolated, formalin-fixed, and paraffin-embedded for subsequent IHC and microdissection. After inclusion in the local

biobank (BD04.002), samples from the CHUM were processed for routine histopathology analysis.

Animals

Animal experiments were carried out using protocols approved by the Animal Care Committee at the University of Ottawa and conforming to or exceeding the standards defined by the Canadian Council on Animal Care. Female C57BL/6 mice (25) were aged up to 33 months such that there were at least six mice per group (0–12 months, 12–20 months, >20 months). Mice were randomly assigned to conventional microisolator cages with plastic huts and corn cob bedding, in groups of five upon weaning. For 4-vinylcyclohexene diepoxide (VCD) treatment, following a 7-day acclimation period, C57BL/6 mice (Charles River Laboratories, strain code: 027) were randomly allocated to two treatment groups (three mice/group). Mice in each cage were randomly allocated to a group that received intraperitoneal injection of PBS or VCD (240 mg/kg in PBS) for 5 simultaneous days. Injections were completed cage by cage. Mice were assessed for wellness by staff of the Animal Care and Veterinary Service on a daily basis, and mice necropsies were done blinded to treatment group. Mice in this study were sacrificed 60 days post-VCD or PBS treatment. Mice were maintained in dedicated rooms for animal breeding (aging) or hazardous chemical procedures (VCD; 21°C, 40%–60% humidity, 12-hour light/dark cycle) and a commercial rodent diet (2018 Teklad Global 18% Protein Rodent Diet, Harlan Laboratories) along with acidified water that was available *ad libitum*. Housing, food, and water were autoclaved prior to use, and all animal handling was performed in a certified ESCO type A2 BSC hood.

Collagen staining and IHC

Histopathologic assessment of murine and human ovaries was performed using hematoxylin and eosin (H&E), Masson's trichrome staining (MTS) or hematoxylin phloxine saffron (HPS) stain, as well as IHC. For assessment of collagen structure using MTS or HPS, ovaries were dichotomized as having mostly linearized collagen (fibrotic) or mostly isotropic collagen structure (nonfibrotic) from visual assessment by two blinded investigators, with concordance between these two assessments used for final classification of fibrotic versus nonfibrotic status. All IHC experiments were done using 5- μ m sections of formalin-fixed paraffin-embedded (FFPE) tissue. Following deparaffinization in xylenes and an alcohol gradient, pressurized antigen retrieval was performed in a citrate buffer (antigen unmasking solution pH 6.0, Dako). Endogenous peroxidase activity was blocked using a 10-minute incubation in 3% H₂O₂. Following PBS washes, immunostaining for murine (m) CD8 (1:400, Abcam No. ab217344), CD4 (1:500, Abcam No. ab183685), FOXP3 (1:500, eBioscience No. 14-5773-82), or human (h) CD8 (1:1,500, Abcam No. ab187279), CD4 (1:500, Abcam No. ab133616), CD68 (1:500, Novus Biologicals No. NB100-683SS), CD206 (1:1,000, Abcam No. ab64693), FOXP3 (1:75, eBioscience 14-4777-82), dipeptidyl-peptidase-4 (DPP4; 1:350, Abcam No. ab61825), or α SMA (1:600, Dako) was performed either 1 hour at room temperature (mCD8, mCD4, hCD8, hCD4, hCD206, α SMA), or overnight at 4°C (mFOXP3, hFOXP3, hCD68, hDPP4). Species appropriate horseradish peroxidase-conjugated secondary antibodies (Vector) were then added for 1 hour at room temperature. Sections were developed in either diaminobenzidine (DAB, Sigma, D8001) for 5 minutes or ImmPACT VIP peroxidase substrate (Vector, SK-4605) for 10 minutes, followed by counterstaining with either hematoxylin (room temperature for 1 minute) or methyl green (55°C for 4 minutes). Sections were then clarified in an alcohol gradient and xylenes and mounted with permount (Thermo Fisher Scientific).

Table 1. Human ovary cohort.

Group	Case No.	Age	BMI ^a	No. of ovarian samples	Metformin use	Gliptin use	T2D status
Premenopausal	1	45	na	1	–	–	–
	2	38	na	1	–	–	–
	3	37	23.1	2	–	–	–
	4	48	26	2	–	–	–
	5	43	27.6	2	–	–	–
	6	21	na	1	–	–	–
	7	28	22.1	1	–	–	–
	8	32	28.4	1	–	–	–
Postmenopausal	9	58	25.2	1	–	–	–
	10	75	20.7	2	–	–	–
	11	60	22.2	1	–	–	–
	12	54	35.3	1	–	–	–
	13	55	na	1	–	–	–
Postmenopausal + metformin use	14	68	35.3	2	+	–	+
	15	69	28.2	2	+	+	+
	16	67	41.7	2	+	–	+
	17	71	25.4	2	+	+	+
	18	53	43.4	2	+	–	+

^aAbbreviations: BMI, body mass index; na, information not available.

Images were acquired using the Scanscope CS2 (Aperio). All assessment and quantification of human samples was performed blinded or by automated image analysis software to remove bias, which was important due to obvious structural change in pre- versus postmenopausal ovaries.

IHC image analysis

Murine image quantification was performed using Aperio ImageScope for cell counts (mCD8, mCD4, mFOXP3) using the count tool and normalizing to ovarian area and also for automated pixel quantification of MTS using hue length: 0.64. Cell counts were performed blinded. Because of the large size of human ovary sections, quantification of hCD68, hCD206, hCD8, hDPP4, h α SMA, hFOXP3, and hCD4 was performed using ImagePro Premier 9.0 software with custom smart segmentation for each stain to quantify cell number or stain area depending on the resolution and clarity of signal. For example, CD4 and CD8 allow for the quantification of cell number, whereas stains of clustering cell types such as DPP4⁺ α SMA⁺ fibroblasts made it challenging to quantify individual cell number and thus areas are presented. To quantify DPP4⁺ α SMA⁺ fibroblasts, the total area of DPP4⁺ signal was multiplied by the ratio of α SMA⁺ signal that coexpresses DPP4⁺ using the parent-child application on ImagePro Premier software. All measurements were normalized to ovarian cortex area (mm²). Representative annotations of an ovarian cortex region were quantified and each double stain is presented in Supplementary Fig. S2B–S2D.

Second-harmonic generation imaging

Unstained paraffinized 5- μ m sections of human ovaries were imaged using second-harmonic generation (SHG) microscopy. Two regions of the ovarian cortex representative of the majority of the cortical collagen architecture by MTS were annotated for imaging. One outlier region representing heterogeneity of collagen architecture was also imaged to determine whether SHG imaging could reveal and match similar features to MTS. Images were acquired using a laser-scanning microscope (Fluoview FVMPE-RS, Olympus) to scan the sample with a Ti:sapphire femtosecond laser (Mai Tai HP, Spectra

Physics). The pulse duration was 150 fs at an 80-MHz pulse frequency, and wavelength was set to 840 nm. The average laser power at the sample was (28 \pm 1) mW. Coherence analysis of collagen fiber orientation in SHG images was performed using the OrientationJ plugin on Fiji software, presented as the average coherence across two regions of the ovarian cortex. Imaging and analysis of SHG were performed blinded.

Ovary microdissection and RNA isolation

FFPE human ovarian samples were first serially sectioned into 10- μ m sections in RNase-free conditions. All sections were immediately stored at -80°C to preserve RNA quality prior to microdissection. Sections were thawed at room temperature prior to automated microdissection using the AVENIO Millisect System (Roche). A serially sectioned hematoxylin-stained reference slide was used to annotate the region of the ovarian cortex to collect. Ovarian surface adhesions and regions near ovulatory follicles (premenopausal ovaries) were excluded from collection. All region annotations were proximal to the ovarian surface epithelium to ensure only ovarian cortex was collected with minimal medulla contamination. Tissue was collected in mineral oil from the same regions in three serially sectioned 10- μ m sections per sample. RNA was then isolated using the RecoverAll Total Nucleic Acid Isolation Kit (Invitrogen, AM1975) as per the manufacturer's instructions and stored at -80°C for downstream applications.

NanoString analysis

RNA quality from microdissected human ovarian samples was assessed using Fragment Analysis (AATI Fragment Analyzer), and concentration was determined using Qubit 3.0 Fluorometer (Thermo Fisher Scientific). All samples met quality control standards as suggested for use with NanoString arrays. NanoString PanCancer Immune Signaling capture and reporter codesets (NanoString, No. 115000132) were mixed with 200 to 300 ng of RNA/sample following concentration of RNA into a 5- μ L volume using the RNA Clean and Concentrator Kit (Zymo, R1015). RNA and codeset solutions were incubated at 65°C for 22 hours. Samples were then run using the

nCounter MAX Analysis System (NanoString) using high-sensitivity settings. Quality control of resultant data was performed using preset standards on nSolver software (NanoString) with all samples passing all quality control standards.

For unsupervised hierarchical clustering and visualization, normalized expression values were \log_2 transformed and housekeeping genes were omitted. Expression values for each gene were then standardized (Z -score transformation) and capped at -3 and 3 to prevent artifactual clustering from a small number of spurious measurements. Samples and genes were separately clustered using Ward's method (ward.d2) from the R package pheatmap. For differential gene expression analysis, normalized expression values were averaged among groups and fold changes (>2 -fold) were derived in all pairwise comparisons using a P value cutoff of 0.05 for significance. For cell type prediction analysis, normalized expression values were assessed using the cell type prediction algorithm in the nCounter Advanced Analysis Software package (version 2.0115) with cell type gene annotations provided in Supplementary Table S4. Cell type scores per sample were averaged within groups. Venn diagrams were produced using the Venny online tool (26).

Gene ontology analysis

All differentially expressed genes ($P < 0.05$) were used to enhance gene ontology (GO) term calling based on the small number of differentially expressed genes in the NanoString dataset. GO term analysis was performed using the DAVID Bioinformatics Resource (27, 28) with an EASE threshold of 0.1 in all pairwise comparisons. Only terms containing more than two genes were included, and resultant P values were \log_{10} transformed.

Statistical analysis

All experiments were performed on a sample size of ≥ 3 as indicated in the figure legends or text. Student t test was used to determine statistical significance of fold change ratios derived from differential gene expression with statistical significance $P < 0.05$. One-way ANOVA was used to determine significance when one variable is presented in three or more groups. Two-way ANOVA was used to determine significance when more than one variable was assessed in three or more groups. Tukey posttest was used in all cases with statistical significance $P < 0.05$. Fisher exact test was used to determine the association between age and fibrotic status with statistical significance $P < 0.05$. t tests, Fisher exact, and ANOVA tests were performed using Prism Software.

Results

Murine age- and ovulation-associated ovarian fibrosis leads to chronic inflammation

We first set out to validate the presence of ovarian fibrosis in aged murine ovaries as previously shown by Briley and colleagues (6). Using a cohort of mice aged from 3 to 33 months old, ovarian stromal collagen content was determined using MTS. Ages were batched from 0 to 12, 12 to 20, and >20 months old. Interestingly, aging resulted in two distinct, mutually exclusive morphologies. Ovarian fibrosis was present in seven of 10 ovaries >20 months old (Fig. 1A and B; Supplementary Fig. S1A–S1C). In contrast, three of 10 ovaries >20 months old did not exhibit fibrosis, instead exhibiting epithelial invaginations that have been termed tubular adenomas in mice, similar to the Ww/Wv model of ovarian aging (Supplementary Fig. S1D; ref. 29). To accelerate and model ovarian aging, VCD was used to induce age-associated changes by destroying ovarian follicles over a

60-day period (30). No ovarian fibrosis was present in VCD-treated ovaries, and the ovarian stroma exhibited a homogenous phenotype lacking the stromal complexity of naturally aged ovaries (Fig. 1A and B; Supplementary Fig. S1E).

To assess the effect of fibrosis on the ovarian microenvironment, we focused on the >20 -month-old ovaries with ovarian fibrosis as assessed by MTS, excluding from further analysis the VCD-treated ovaries and aged ovaries >20 months old with tubular adenomas. To determine whether ovarian fibrosis correlates with the infiltration of immune subtypes commonly found in sites of chronic inflammation, IHC detection of CD8, CD4, and FOXP3 was performed (31–33). Enhanced populations of CD8⁺, CD4⁺, and FOXP3⁺ T cells were present in serial sections of fibrotic ovaries >20 months old compared with ovaries aged 0 to 20 months (Fig. 1C–H).

Metformin abrogates age-associated ovarian fibrosis in postmenopausal human ovaries

To determine whether ovarian fibrosis also develops during human aging, we accrued a cohort of human ovaries ranging in age from 21 to 75 years old (Table 1). Given the ovarian cancer risk reduction observed with metformin use in women who have T2D and the role of metformin in suppressing fibrosis in other tissues (21, 34), we also accrued postmenopausal ovaries from patients who were taking metformin for T2D treatment at the time of oophorectomy. Among patients taking metformin, two of five patients were also prescribed gliptins that inhibit the enzymatic function of DPP4 and promote the action of incretin hormones to improve glycemic control in T2D (Table 1; refs. 35, 36). For downstream analyses, each ovary from a patient was treated as independent to determine whether human ovaries age synchronously, which was in part due to evidence that some types of ovarian cancer often present unilaterally and that the frequency of contralateral ovulations becomes disproportionate with age (23, 24).

The analysis focused on the ovarian cortex region underlying the surface epithelium and tunica albuginea as this region is where epithelial inclusion cysts form (putative sites of cancer origin) and the likely site of serous tubal intraepithelial carcinoma migration into the ovary in the early stages of ovarian cancer. Classic H&E staining has low resolution for delineating collagen organization with no obvious differences among groups (Fig. 1I). In contrast, MTS, which specifically stains collagens, revealed isotropic collagen organization in premenopausal ovaries and in postmenopausal ovaries with metformin use (hereafter referred to as metformin ovaries), which is characteristic of normal tissue collagen organization (Fig. 1J). In contrast, postmenopausal ovaries without metformin use exhibited anisotropic (linearized) collagen architecture (Fig. 1J) consistent with age-related changes in collagen organization and characteristic of organ fibrosis (reviewed in refs. 37, 38).

SHG imaging is a highly sensitive modality to quantify collagen structure at a submicron resolution based on the noncentrosymmetric nature of collagen proteins (39–41). To quantify collagen organization, SHG images of the ovarian cortex were used to calculate the coherence of collagen fiber directionality, with increased coherence representing more anisotropic collagen structure while less coherence represents isotropic collagen (Fig. 1K and L). Consistent with the structure revealed by MTS (Fig. 1J), premenopausal and metformin ovaries have less coherence, whereas postmenopausal ovaries have increased collagen coherence (Fig. 1L). The term “fibrotic” was assigned to ovaries with collagen linearization as seen using MTS, with SHG values within each case adding support to our classification. These data show

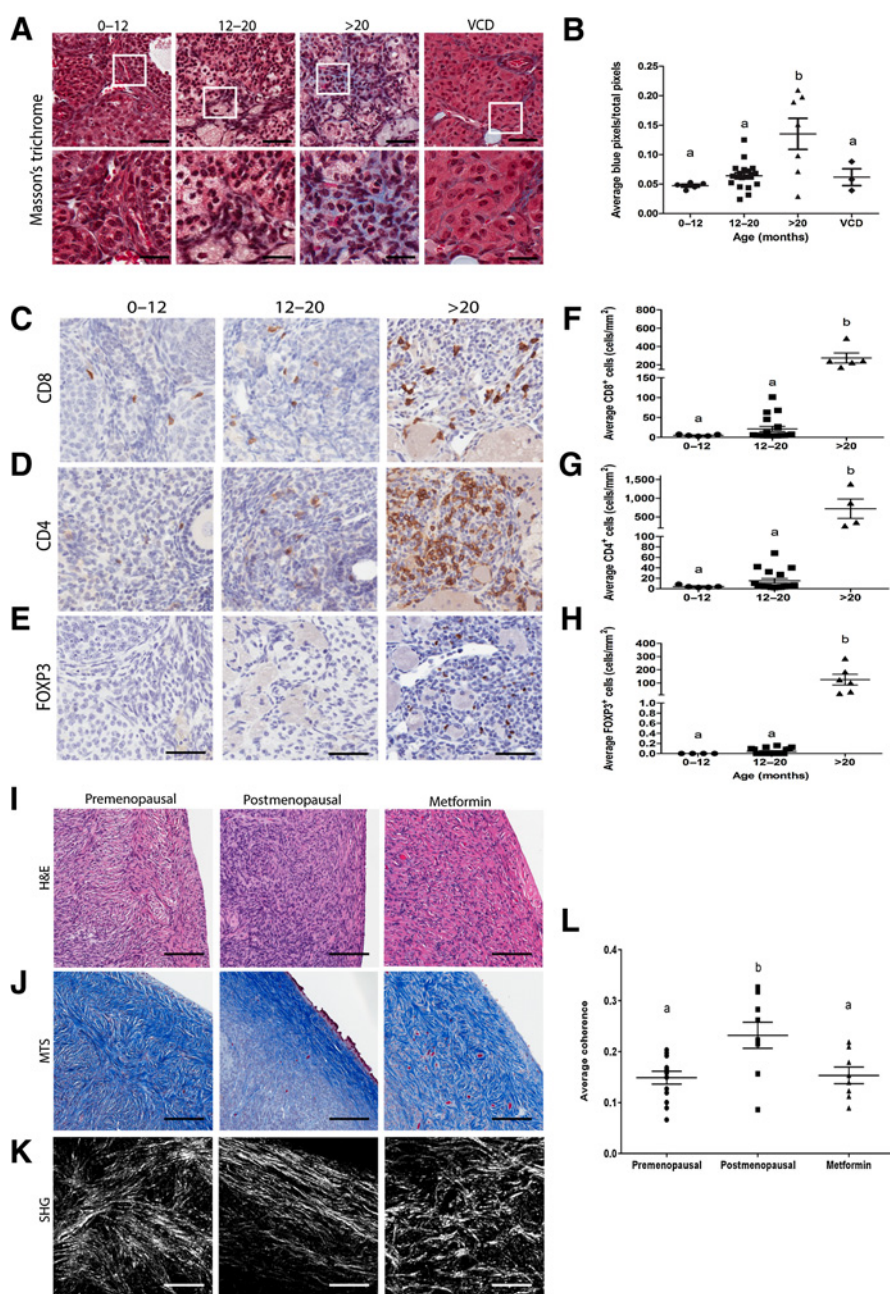


Figure 1.

Age-associated fibrosis occurs in murine and human ovaries. **A–H**, Ovaries were isolated from C57BL/6 mice over an aging time course. Ages were batched from 0 to 12 ($n = 5$), 12 to 20 ($n = 19$), and >20 ($n = 7$) months. Five-week-old mice were given intraperitoneal injection of 4-vinylcyclohexene diepoxide (VCD, 240 mg/kg) daily for 5 days ($n = 3$) and ovaries collected after two months. **A**, Representative images of MTS for each age batch and VCD-treated ovaries. Collagens, blue; erythrocytes and fibrin, red; nuclei, purple. White box indicates region of ovary presented in the bottom. Scale bars, 50 μm (top) and 25 μm (bottom). **B**, Quantification of collagen deposition. Total blue pixels (hue value 0.64) were normalized to total pixel counts and averaged within groups. **C–E**, Representative images of IHC detection of CD8, CD4, and FOXP3 are presented. Scale bar, 50 μm . **F–H**, Quantification of CD8, CD4, and FOXP3⁺ cell numbers normalized to ovarian area. **A–H**, All data represent the average of three sections (50 μm apart). **I**, H&E staining of human ovarian cortex. **J**, MTS of human ovarian cortex with collagens, blue; erythrocytes and fibrin, red; and nuclei, purple. **I** and **J**, Scale bar, 125 μm . **K**, Second-harmonic generation microscopy of human ovarian cortex in serially sectioned tissue. Scale bar, 64 μm . **L**, Quantification of collagen anisotropy. Coherence of collagen fiber directionality was determined using the OrientationJ plugin on Fiji software. The results from two SHG images per sample were averaged and group averages are presented, premenopausal ($n = 13$), postmenopausal ($n = 9$), and metformin ($n = 8$). One-way ANOVA with Tukey posttest was used to determine significance with a,b indicating significance between groups ($P < 0.05$).

that age-associated ovarian fibrosis develops in human ovaries similar to that seen in aged murine ovaries (Fig. 1A and B; Supplementary Fig. S1), with metformin use associated with abrogation of this aging phenotype.

A small independent aging validation cohort of premenopausal ($n = 3$) and postmenopausal ($n = 6$) ovaries was acquired (Table 2). Assessment of fibrosis in this cohort supports our initial findings of age-associated ovarian fibrosis with only one of three premenopausal cases exhibiting fibrosis, whereas five of six postmenopausal cases had fibrosis (Table 2). Across both original and independent cohorts, three of 11 premenopausal ovaries were fibrotic, whereas nine of 11 postmenopausal ovaries were fibrotic, revealing a significant association between age and fibrosis (Fisher exact test, $P = 0.03$).

Menopausal status stratifies ovarian cortex gene expression

We next determined whether ovarian fibrosis correlates with altered gene expression in the ovarian cortex. RNA was isolated from the human ovarian cortex using automated microdissection (Supplementary Fig. S2A). Isolated RNA was run on NanoString PanCancer Immune Profiling arrays that contain 770 immunoregulatory genes, including genes that are involved in regulating the stromal microenvironment such as *TGF β* and collagens. Unsupervised hierarchical clustering revealed that ovarian samples generally cluster according to menopausal status (Fig. 2A). All but one pair of samples derived from contralateral ovaries within the same case clustered together, highlighting low intracase variability in immune-related RNA expression. All metformin ovaries and five of seven premenopausal cases lacked fibrosis. In contrast, four of six fibrotic ovaries (cases

Table 2. Summary of histopathologic assessment of collagen architecture in an independent human ovary validation cohort.

Group	Case No.	Age	Metformin	Fibrosis ^a (0 = no, 1 = yes)	Total fibrotic ovaries by group
Premenopausal	19	45	—	0	1/3 (33%)
	20	42	—	0	
	21	41	—	1	
Postmenopausal	22	68	—	1	5/6 (83%)
	23	82	—	0	
	24	66	—	1	
	25	63	—	1	
	26	63	—	1	
	27	71	—	1	

^aFibrosis indicates the ovarian cortex has regions of linearized collagen.

1, 2, 9, and 11) and one ovarian sample from case 10 formed an independent cluster within the third branchpoint (Fig. 2A). In the two premenopausal ovaries that clustered with postmenopausal ovaries, both exhibited linearized collagen by SHG and MTS, and were deemed fibrotic (case 1 and 2).

Metformin use regulates profibrotic and complement pathway gene expression

We next aimed to determine whether ovarian fibrosis leads to inflammation and tumor-permissive gene expression signatures characteristic of a premetastatic niche. For differential gene expression analysis of the NanoString Immune Signaling array dataset, samples were grouped according to fibrotic status and metformin use as indicated in Fig. 2A, comparing nonfibrotic samples ($n = 7$), fibrotic samples ($n = 7$), and the metformin ovaries, which all lack fibrosis ($n = 8$). Venn diagrams representing uniquely or shared up- and downregulated genes among all pairwise comparisons are presented with 111 upregulated and 24 downregulated genes in fibrotic versus nonfibrotic ovaries, 237 upregulated and 45 downregulated genes in metformin versus nonfibrotic ovaries, and 57 upregulated and 36 downregulated genes in metformin versus fibrotic ovaries (Fig. 2B). Up to the top five up- and downregulated genes in all pairwise comparisons are highlighted (Fig. 2C). In metformin ovaries compared with either fibrotic or nonfibrotic ovaries, *DPP4* was the most downregulated gene, whereas *ARG2* was the most upregulated gene, suggesting these genes may be key targets of metformin activity. Interestingly, four of eight ovarian samples in the metformin group were from patients also taking *DPP4* inhibitors (gliptins). In addition to the effect of *DPP4* inhibition on incretin hormones, *DPP4* has also been identified as a marker of a hyperactive profibrotic fibroblasts (42), suggesting gliptin use may inhibit profibrotic processes. Gliptins function to inhibit the enzymatic function of *DPP4* and not transcription (43). Consistent with this, when differential gene expression analysis was performed omitting samples with gliptin use, *DPP4* was still among the most downregulated gene in metformin ovaries (Supplementary Fig. S3), suggesting that *DPP4* downregulation is consistent in metformin ovaries and not solely an effect of gliptin, although synergy may occur.

Up to 10 significant GO terms among all pairwise comparisons are presented (Fig. 2D) with details of each GO term presented in Supplementary Tables S1–S3. Defense response, lymphocyte chemotaxis, and cellular response to TNF are among upregulated GO terms in fibrotic ovaries, while downregulated terms include regulation of

innate immune response, stimulatory C-type lectin receptor signaling, and T-cell receptor signaling pathway, in comparison with nonfibrotic ovaries (Fig. 2D). Similar to fibrotic ovaries, immune response, inflammatory response, T-cell activation, and complement activation are upregulated in metformin compared with nonfibrotic ovaries, suggesting a more inflammatory environment is present in both fibrotic and metformin ovaries that are largely representative of postmenopausal samples within the cohort (Fig. 2D). Downregulated GO terms in metformin versus nonfibrotic ovaries include peptide cross-linking, platelet-derived growth factor receptor signaling pathway, and regulation of complement activation (Fig. 2D). Compared with fibrotic ovaries, metformin ovaries have elevated expression of genes associated with complement activation (Fig. 2C), and downregulation of GO terms including response to wounding (Fig. 2D). Intriguingly, among genes downregulated in metformin versus fibrotic ovaries, *NRP1*, *DPP4*, and *TGFβ2* are known to promote fibrosis and contribute to premetastatic niche formation (10, 42, 44). In addition, numerous complement pathway proteins are downregulated in metformin ovaries including *C3* that has been implicated in promoting both fibrosis and premetastatic niche formation (45–48). These data are suggestive of proinflammatory signaling in both fibrotic and metformin ovaries in comparison with nonfibrotic ovaries, yet there is a downregulation of genes implicated in fibrosis and premetastatic niche formation in metformin ovaries.

Metformin alters the ovarian immune landscape

Given the increase in proinflammatory gene expression in both fibrotic and metformin ovaries, we next sought to profile the immune landscape of the ovarian cortex and validate gene expression signatures related to fibrotic signaling. Estimation of immune cell type abundance was performed using the NanoString nSolver cell type prediction algorithm that assigns gene sets to specific immune subsets (annotations provided in Supplementary Table S4). Cell types predicted to significantly change among nonfibrotic, fibrotic, and metformin ovaries included CD8 T cells, regulatory T cells (Treg), $\gamma\delta$ T cells, B cells, aDCs, natural killer (NK) CD56 bright cells, M1 macrophages, and eosinophils (Fig. 3A), whereas CD45, total T cells, T helper, Th1, Th2, effector memory T cells (Tem), central memory T cells (Tcm), Th17, total dendritic cells (DC), induced DCs, total NK cells, CD56^{dim} NK cells, M2 macrophages, neutrophils, and mast cells were predicted to be unchanged in abundance (Supplementary Fig. S4A).

Because of the role of macrophages in promoting tissue remodeling and repair (reviewed in ref. 49), along with metformin ovaries predicted to have increased M1-like macrophage abundance (Fig. 3A), we sought to validate the abundance of M1-like and M2-like macrophages. M1 macrophages promote early inflammation during a wound healing response and contribute to functional immunosurveillance, while alternatively activated immunosuppressive M2 macrophages promote wound healing and resolution, but can also promote premetastatic niche formation (49–51). In addition, chronic inflammation and unhealed wounding can stabilize M2 polarization leading to enhanced fibrogenesis (52). Using IHC detection of M2-like marker CD206 (MRC1) and pan-macrophage marker CD68, fibrotic ovaries were found to have an increased CD206:CD68 ratio compared with both nonfibrotic and metformin ovaries, showing ovarian fibrosis correlates with enhanced M2-like polarization (Fig. 3B and C). In contrast, metformin use correlated with M1-like polarization as shown by a decrease in the CD206:CD68 ratio (Fig. 3C). We next validated the abundance of CD8⁺ T cells as they were predicted to increase in fibrotic and metformin ovaries. Surprisingly, fibrotic ovaries had increased CD8⁺ T-cell infiltration while metformin ovaries had levels

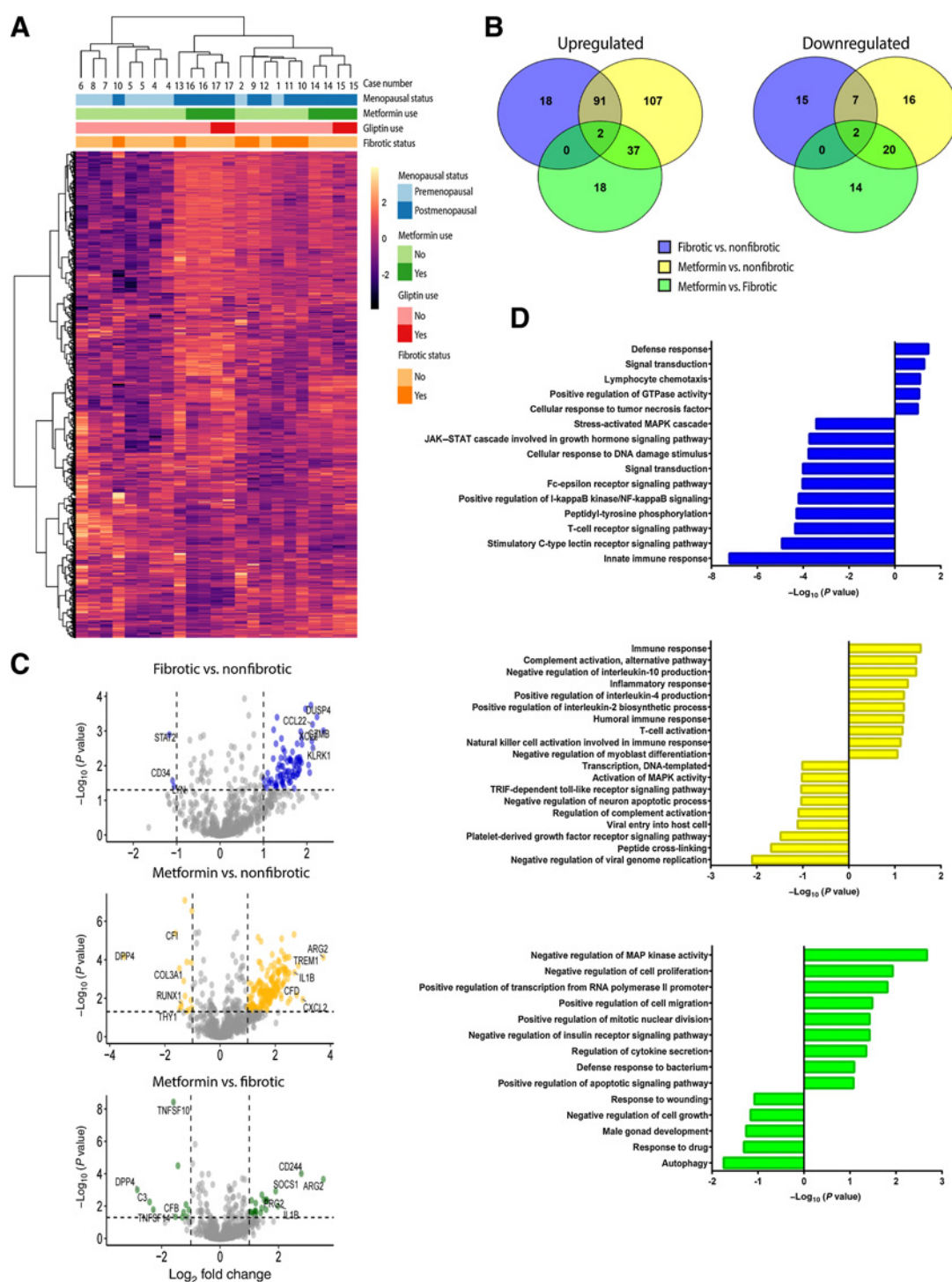


Figure 2. Menopausal status stratifies ovarian cortex gene expression profiles. **A**, Unsupervised hierarchical clustering of contralateral case samples of premenopausal ($n = 9$), postmenopausal ($n = 6$), and metformin ($n = 8$) ovaries is presented. Normalized RNA expression values were \log_2 transformed and housekeeping genes omitted. Case numbers and annotations for menopausal status, metformin use, and gliptin use correspond to **Table 1**. Fibrotic status was determined histologically by MTS and collagen fiber coherence by SHG imaging. **B**, Venn diagrams depicting the number of shared or uniquely up- and downregulated regulated genes in all pairwise comparisons. **C**, Fold changes in RNA expression among all pairwise comparisons are presented. Up to the top five upregulated and downregulated genes among all pairwise comparisons are labeled. **D**, Upregulated and downregulated GO terms in all pairwise comparisons are presented.

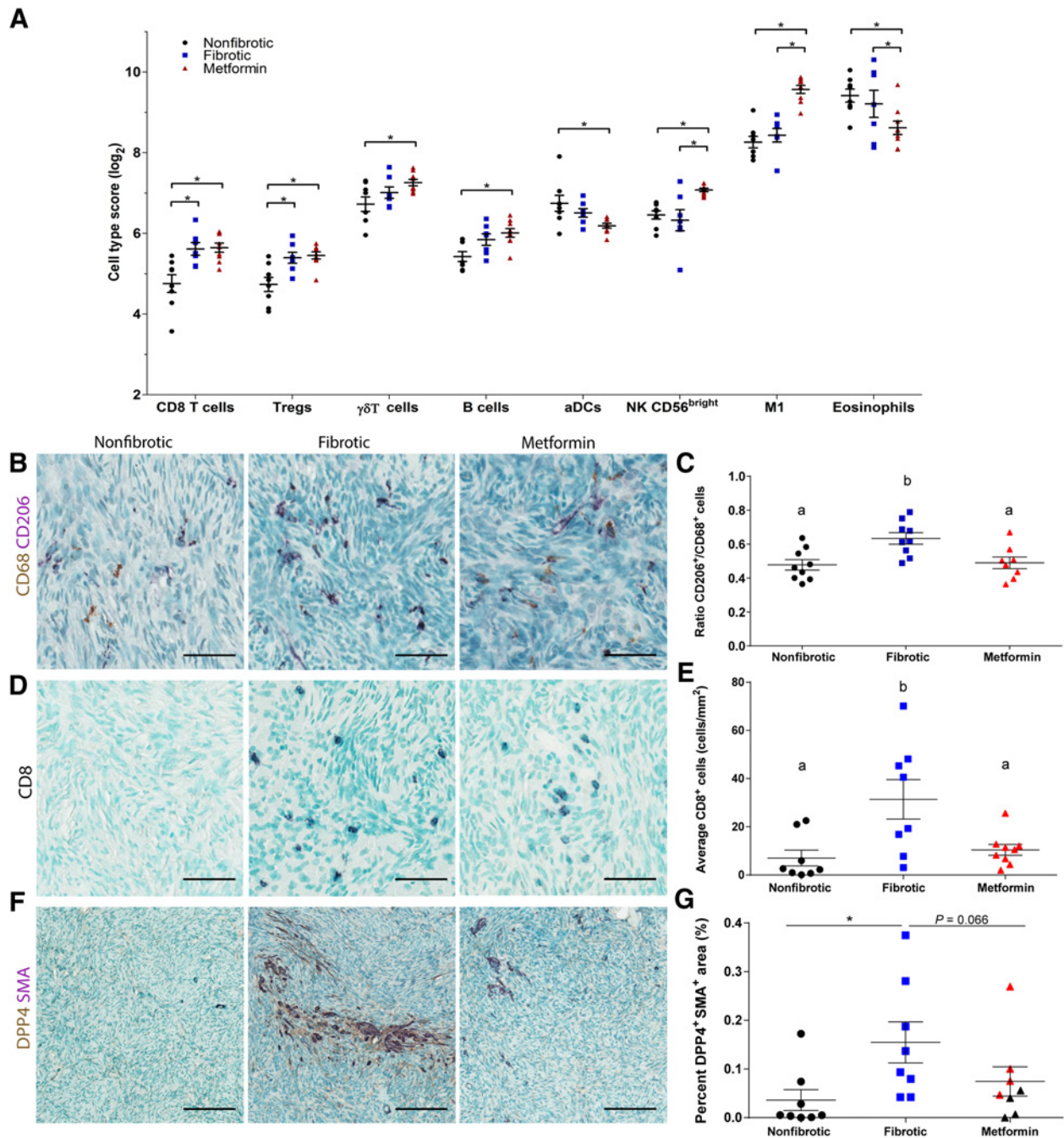


Figure 3. Metformin use alters the immune and stromal landscape of the ovarian cortex. **A**, Cell type prediction scores for nonfibrotic ($n = 8$), fibrotic ($n = 7$), and metformin ($n = 8$) ovaries. Average log-scale expression based on a modified Pearson correlation coefficient of cell type-specific gene sets is presented. Two-way ANOVA with Tukey posttest was used to determine significance with *, $P < 0.05$. **B**, Double IHC detection of pan-macrophage marker CD68 (brown) and M2 macrophage marker CD206 (purple). **C**, Quantification of the ratio of CD206⁺/CD68⁺ cells normalized to tissue area (mm²). **D**, IHC detection of CD8. **E**, Quantification of CD8⁺ cells normalized to tissue area (mm²) was averaged among groups. **F**, Double IHC detection of DPP4 (brown) and α SMA (SMA, purple). **G**, Quantification of the percentage of DPP4⁺SMA⁺ area (μ m²) normalized to tissue area (μ m²) was averaged among groups. All sections were counterstained with methyl green, and all images are representative of each sample and group. Black triangles indicate samples with combined metformin and gliptin use, whereas red triangles indicate metformin use alone. P value presented refers only to samples with combined metformin and gliptin use compared with fibrotic samples. **B**, **D**, and **F**, Representative images of nonfibrotic ($n = 8-9$), fibrotic ($n = 8-9$), and metformin ($n = 8$) ovaries are shown. One-way ANOVA with Tukey posttest was used to determine significance with **C**, **E** a, b, or **G**. * indicates significance ($P < 0.05$) between groups. **B** and **D**, Scale bar, 50 μ m. **F**, Scale bar, 125 μ m.

Downloaded from <http://aacrjournals.org/clinccancerres/article-pdf/26/3/632/2064644/632.pdf> by University of Ottawa user on 17 February 2023

similar to nonfibrotic ovaries (Fig. 3D and E), suggesting that metformin use may abrogate features of chronic inflammation in postmenopausal ovaries. In contrast, FOXP3⁺ Tregs were predicted to be upregulated in fibrotic and metformin ovaries, although no significant differences were found among groups (Supplementary Fig. S4C and S4E).

Enhanced fibroblast activation in fibrotic ovaries

Given the downregulation of *DPP4* in metformin ovaries (Fig. 2C) and recent evidence that DPP4⁺ fibroblasts are profibrotic (42), we sought to determine the effects of aging and metformin use on DPP4⁺ fibroblasts in the ovarian cortex. Using double IHC detection of DPP4 and fibroblast marker α SMA, fibrotic ovaries have increased DPP4⁺ α SMA⁺ fibroblasts compared with nonfibrotic ovaries (Fig. 3F and G). There was no decrease in DPP4⁺ α SMA⁺ fibroblasts in metformin ovaries compared with fibrotic ovaries ($P = 0.15$ by one-way ANOVA; Fig. 3G). However, within the metformin group, samples from patients with combined metformin and gliptin use (Table 1, cases 15 and 17) had a trend towards reduction in DPP4⁺ α SMA⁺ fibroblasts when compared with fibrotic ovaries (Fig. 3G, black triangles, $P = 0.066$). These data further support the development of ovarian fibrosis in postmenopausal ovaries.

Discussion

Organ fibrosis has become an established fertile “soil” that is permissive to tumorigenesis and metastasis (8–10). The restructuring of ECM components in fibrosis such as collagens and fibronectin provide mechanosensory cues that facilitate cancer cell invasion (37, 53). In addition, chronic inflammation, which is characteristic of fibrosis, provides cytokines that enhance fibroblast activation and establish a microenvironment that promotes metastases (7, 37, 54). Ovarian cancers are age-associated cancers with the median age of diagnosis of 63 years old, although the reasons for this have been largely understudied. Many of the changes found in fibrosis are characteristic of normal aging tissues. A recent study by Loughran and colleagues has shown that aging promotes enhanced metastasis within the peritoneal cavity following intraperitoneal injection of ID8-*Trp53*^{-/-} cells, including enhanced metastasis to the ovary (55). In addition, age-associated fibrosis was shown to occur in murine ovaries (6). Here, we validated the presence of age-associated murine ovarian fibrosis with fibrosis present in 70% of mice >20 months old. In contrast, 30% of mice >20 months old had no signs of ovarian fibrosis and exhibited loss of follicles and tubular adenomas similar to the *Wv/Wv* model, a phenotype previously suggested to increase cancer risk (29, 56). This highlights the possibility of multiple forms of ovarian aging, which may have differential cancer risk based on the resultant microenvironment. Interestingly, no fibrosis was present in VCD-treated ovaries, suggesting that the fibrotic phenotype may be due to cumulative ovulations instead of a direct effect of follicle loss. Our study translates these murine findings and provides novel evidence of age-associated ovarian fibrosis in postmenopausal human ovaries using MTS, HPS, or SHG imaging within two independent patient cohorts.

Two studies have shown a protective effect of metformin use on ovarian cancer incidence in women with T2D (21, 57); however, a conflicting outcome was reported from a study profiling a different patient cohort (58). Interestingly, in the study done by Tseng and colleagues that profiled 640,193 Taiwanese women with T2D, the overall risk in women with T2D not taking metformin (never-user) was 146.4 per 100,000 person-years compared with 49.4 for those who

have taken metformin (ever-user; ref. 21). In contrast, Urpilainen and colleagues found risk to be 39.3 and 41.1 per 100,000 person-years for never-user and ever-users, respectively, among their Finnish cohort (58). Aside from the small sample size of the Finnish cohort with only 303 of 137,643 patients having ovarian cancer, it is curious that the never-user risk among the Finnish cohort (39.3) is much lower than the never-user risk among the Taiwanese cohort (146.4), suggesting that the Finnish T2D population's overall risk is lower than the risk among Taiwanese women with T2D (21). Indeed, a robust meta-analysis performed by Wen and colleagues showed that metformin use lowers the risk of ovarian cancer in Asian but not Caucasian populations (59). More global studies are needed to determine the efficacy of metformin use in ovarian cancer risk reduction within the T2D population, with particular effort needed to stratify the effect of metformin use on risk reduction by ovarian cancer subtype, which is currently lacking among the published epidemiologic studies. In addition, no mechanisms for the observed ovarian cancer risk reduction with metformin use have been elucidated, with observed effects hypothesized to be due to the actions of metformin on metabolism. Here, we show that metformin use in postmenopausal women (metformin ovaries) may reverse or prevent fibrosis, as shown by MTS and SHG imaging. A major limitation of this study was that all ovarian samples provide a snapshot at a single time point, limiting our ability to assess the level of ovarian fibrosis prior to metformin use within each case in our cohort. More studies are required to determine whether metformin prevents collagen anisotropy or reverses it once fibrosis is established. Limitations to this study also include the small sample size of our patient cohorts and a lack of information on parity and oral contraceptive use such that the contribution of cumulative ovulations to age-associated human ovarian fibrosis could not be determined. In addition, future studies would benefit from techniques that allow for robust coexpression of immune markers such as flow cytometric analysis of freshly dissociated ovarian tissues to enumerate more complex immune cell populations.

Moreover, given that two ovaries within the fibrotic group are premenopausal, whereas all metformin ovaries are postmenopausal, we accounted for the possibility that the hormone milieu of these two samples may alter gene expression in the metformin versus fibrotic pairwise comparison. In a restricted comparison of metformin versus no metformin postmenopausal ovaries, the top five upregulated genes (*CD244*, *ARG2*, *FOXJ1*, *IL10*, and *IL1B*) and top five downregulated genes (*TNFSF14*, *C3*, *CFB*, *DPP4*, and *RORC*) are very similar to the main comparison of metformin versus fibrotic ovaries (up: *ARG2*, *CD244*, *IL1B*, *SOCS1*, *PRG2*, down: *DPP4*, *TNFSF14*, *C3*, *CFB*, *TNFSF10*), which suggests minimal contribution of the hormone milieu to the expression profile of fibrotic ovaries.

Among differentially expressed genes in metformin compared with fibrotic ovaries, *DPP4* was the most downregulated gene. *DPP4* marks a lineage of profibrotic fibroblasts, and we found DPP4⁺ α SMA⁺ fibroblasts were significantly upregulated in fibrotic ovaries compared with nonfibrotic ovaries. There was a trend toward higher levels of DPP4⁺ α SMA⁺ fibroblasts in fibrotic ovaries compared with metformin ovaries with noted gliptin use ($P = 0.066$). These results highlight a possible synergistic effect with metformin and gliptin use in the regulation of ovarian fibrosis, warranting further, more robust exploration of this drug combination on the regulation of profibrotic fibroblasts and ovarian fibrosis. The gene expression profile along with the isotropic collagen architecture in metformin ovaries suggests that metformin use abrogates features characteristic of a tumor-permissive niche within the ovary (10). Interestingly, even though evidence shows that contralateral ovulations can be unequal as women

age (24), this did not have a notable effect on immune-related gene expression between most pairs of ovaries. All paired ovarian samples clustered together with the exception of case 10. Future studies should aim to use more robust methods such as RNA sequencing to further examine whether contralateral ovaries age similarly.

Macrophages are key players in mediating tissue inflammation upon injury, and also in wound healing and resolution (49). Non-fibrotic and metformin ovaries had a reduced CD206:CD68 ratio when compared with fibrotic ovaries, suggesting metformin may affect macrophage polarization either directly, or through regulating ovarian fibrosis that in turn alters polarization. In addition, T2D and obesity have been shown to promote M1 macrophage polarization in adipose tissue (60), a phenotype that may extend to other sites such as the ovary. Therefore, this enhanced M1-like polarization in metformin ovaries, all of which are T2D, could be a function of T2D and/or obesity instead of an effect of metformin use. Nonetheless, enhanced M1-like polarization in metformin ovaries suggests enhanced tissue immunosurveillance. In contrast, enhanced M2-like polarization in fibrotic ovaries is suggestive of a chronic inflammatory state permissive to tumorigenesis (61). Consistent with these findings, metformin use downregulated complement pathway protein C3, which has been implicated in fibrosis, the establishment of a premetastatic niche within the cerebrospinal fluid, and in the promotion of M2 polarization, such that increased C3 promotes M2 polarization during tumor progression (46–48, 62). In addition to enhanced M1 polarization, the cytokine milieu upregulated in metformin ovaries (*CCL26*, *IL10*, *VEGFA*) suggests enhanced M2c polarization among the CD206⁺ population, which are a subset of M2 macrophages involved in the resolving fibrosis (49, 63). This could indicate that metformin use may also promote the resolution phase of tissue repair. More mechanistic studies will be required to tease out the contribution of various macrophage populations to ovarian aging.

Interestingly, some premenopausal samples (cases No. 1 and 2) had evidence of fibrosis by SHG and MTS and clustered with fibrotic postmenopausal ovaries. Of these two cases, case No. 2 was deemed high-risk due to family history, but did not carry a *BRCA* mutation. This may suggest that factors beyond age may accelerate the development of ovarian fibrosis, meriting more study into the association between ovarian fibrosis and ovarian cancer risk factors such as high-risk mutations.

Taken together, this study provides a possible mechanism for the demonstrated ovarian cancer risk reduction with metformin use in women with T2D through the abrogation of microenvironmental cues that facilitate cancer growth and metastasis. This study positions metformin use in the context of regulating fibrosis instead of solely

affecting cell metabolism to reduce cancer risk. Finally, this study offers novel insights into the age- and ovulation-associated risk of ovarian cancer, introducing modulation of ovarian fibrosis as a possible new frontier for ovarian cancer prevention.

Disclosure of Potential Conflicts of Interest

B. Lo is an employee/paid consultant for Novartis, Bayer, Roche, and AstraZeneca and reports receiving commercial research grants from Roche and Amgen. No potential conflicts of interest were disclosed by the other authors.

Authors' Contributions

Conception and design: C.W. McCloskey, B.C. Vanderhyden

Development of methodology: C.W. McCloskey, B. Lo

Acquisition of data (provided animals, acquired and managed patients, provided facilities, etc.): C.W. McCloskey, B.S. Kelly, F. Azzi, C.H. Allen, A. Forsyth, J. Upham, D.A. Gray, R.W. Boyd, B. Lo, D. Trudel, M.K. Senterman, B.C. Vanderhyden

Analysis and interpretation of data (e.g., statistical analysis, biostatistics, computational analysis): C.W. McCloskey, D.P. Cook, F. Azzi, D. Trudel, B.C. Vanderhyden

Writing, review, and/or revision of the manuscript: C.W. McCloskey, D.P. Cook, F. Azzi, J. Upham, D.A. Gray, D. Trudel, M.K. Senterman, B.C. Vanderhyden

Administrative, technical, or material support (i.e., reporting or organizing data, constructing databases): K.J. Rayner, R.W. Boyd, B.C. Vanderhyden

Study supervision: R.W. Boyd, M.K. Senterman, B.C. Vanderhyden

Other (facilitated SHG imaging and data analysis): S. Murugkar

Other [anatomic pathologist on this project, provided tissue specimens (ovaries, according to the parameters of the study), performed histologic interpretation of changes seen in the ovaries, reviewed histologic changes with the principal author, reviewed manuscript and provided changes (particularly those related to the pathology portions of the manuscript), and responded to questions concerning histologic changes posed by one reviewer]: M.K. Senterman

Acknowledgments

We would like to acknowledge and honor the late Margaret Craig, whose generous support funded the majority of this study. Ovarian tumor banking at the CRCHUM was supported by the Banque de tissus et de données de the Réseau de recherche sur le cancer of the FRQS affiliated with the Canadian Tumor Repository Network (CTRNet). We would also like to acknowledge the Department of Pathology at the Ottawa Hospital for their hard work in preparing the ovarian cortex samples. We thank Michele Geoffrion from the Ottawa Heart Institute for her help with Nano-String arrays and Aditya Babu for his help with the SHG data acquisition. This project received funding from the Canadian Institutes of Health Research (MOP136829). C.W. McCloskey is funded by a Vanier Canada Graduate Scholarship and D.P. Cook is funded by a CIHR Doctoral Research Award.

The costs of publication of this article were defrayed in part by the payment of page charges. This article must therefore be hereby marked *advertisement* in accordance with 18 U.S.C. Section 1734 solely to indicate this fact.

Received February 18, 2019; revised June 2, 2019; accepted October 4, 2019; published first October 9, 2019.

References

- Auersperg N. The origin of ovarian cancers—hypotheses and controversies. *Front Biosci (Schol Ed)* 2013;5:709–19.
- National Cancer Institute. *Cancer Stat Facts: Ovarian Cancer*. 2018[cited 2018 Aug 15]. Available from: <https://seer.cancer.gov/statfacts/html/ovary.html>.
- Fathalla MF. Incessant ovulation and ovarian cancer – a hypothesis re-visited. *Facts Views Vis Obgyn* 2013;5:292–7.
- Fleming JS, Beaugié CR, Haviv I, Chenevix-Trench G, Tan OL. Incessant ovulation, inflammation and epithelial ovarian carcinogenesis: revisiting old hypotheses. *Mol Cell Endocrinol* 2006;247:4–21.
- Rebbeck TR, Mitra N, Wan F, Sinilnikova OM, Healey S, McGuffog L, et al. Association of type and location of BRCA1 and BRCA2 mutations with risk of breast and ovarian cancer. *JAMA* 2015;313:1347–61.
- Briley SM, Jasti S, McCracken JM, Hornick JE, Fegley B, Pritchard MT, et al. Reproductive age-associated fibrosis in the stroma of the mammalian ovary. *Reproduction* 2016;152:245–60.
- Langley RR, Fidler IJ. The seed and soil hypothesis revisited - the role of tumor-stroma interactions in metastasis to different organs. *Int J Cancer* 2011;128:2527–35.
- Olaso E, Santisteban A, Bidaurrezaga J, Gressner AM, Rosenbaum J, Vidal-Vanaclocha F. Tumor-dependent activation of rodent hepatic stellate cells during experimental melanoma metastasis. *Hepatology* 1997;26:634–42.
- Jacobs TW, Byrne C, Colditz G, Connolly JL, Schnitt SJ. Radial scars in benign breast-biopsy specimens and the risk of breast cancer. *N Engl J Med* 1999;340:430–6.
- Cox TR, Erler JT. Molecular pathways: connecting fibrosis and solid tumor metastasis. *Clin Cancer Res* 2014;20:3637–43.
- Cox TR, Bird D, Baker A-M, Barker HE, Ho MW-Y, Lang G, et al. LOX-mediated collagen crosslinking is responsible for fibrosis-enhanced metastasis. *Cancer Res* 2013;73:1721–32.

12. Nielsen SR, Quaranta V, Linford A, Emeagi P, Rainer C, Santos A, et al. Macrophage-secreted granulin supports pancreatic cancer metastasis by inducing liver fibrosis. *Nat Cell Biol* 2016;18:549–60.
13. Li W, Wang H, Wang J, Lv F, Zhu X, Wang Z. Ovarian metastases resection from extragenital primary sites: outcome and prognostic factor analysis of 147 patients. *BMC Cancer* 2012;12:278.
14. Bigorie V, Morice P, Duillard P, Antoine M, Cortez A, Flejou JF, et al. Ovarian metastases from breast cancer: report of 29 cases. *Cancer* 2010;116:799–804.
15. Karnezis AN, Cho KR, Gilks CB, Pearce CL, Huntsman DG. The disparate origins of ovarian cancers: pathogenesis and prevention strategies. *Nat Rev Cancer* 2017;17:65–74.
16. Choi SM, Jang A-H, Kim H, Lee KH, Kim YW. Metformin reduces bleomycin-induced pulmonary fibrosis in mice. *J Korean Med Sci* 2016;31:1419–25.
17. Wang M, Weng X, Guo J, Chen Z, Jiang G, Liu X. Metformin alleviated EMT and fibrosis after renal ischemia-reperfusion injury in rats. *Ren Fail* 2016;38:614–21.
18. Kita Y, Takamura T, Misu H, Ota T, Kurita S, Takeshita Y, et al. Metformin prevents and reverses inflammation in a non-diabetic mouse model of non-alcoholic steatohepatitis. *PLoS One* 2012;7:e43056.
19. Ursini F, Grembale RD, D'Antona L, Gallo E, D'Angelo S, Citraro R, et al. Oral metformin ameliorates bleomycin-induced skin fibrosis. *J Invest Dermatol* 2016;136:1892–4.
20. Xiao H, Ma X, Feng W, Fu Y, Lu Z, Xu M, et al. Metformin attenuates cardiac fibrosis by inhibiting the TGFbeta1-Smad3 signalling pathway. *Cardiovasc Res* 2010;87:504–13.
21. Tseng C-H. Metformin reduces ovarian cancer risk in Taiwanese women with type 2 diabetes mellitus. *Diabetes Metab Res Rev* 2015;31:619–26.
22. Shi J, Liu B, Wang H, Zhang T, Yang L. Association of metformin use with ovarian cancer incidence and prognosis: a systematic review and meta-analysis. *Int J Gynecol Cancer* 2019;29:140–6.
23. Chen VW, Ruiz B, Killeen JL, Cot TR, Wu XC, Correa CN, et al. Pathology and classification of ovarian tumors. *Cancer* 2003;97:2631–42.
24. Fukuda M, Fukuda K, Andersen CY, Byskov AG. Characteristics of human ovulation in natural cycles correlated with age and achievement of pregnancy. *Hum Reprod* 2001;16:2501–7.
25. Fotheringham AP, Davies I. Age related accumulation of intranuclear membranous inclusions in female mice. *J Am Aging Assoc* 1980;3:1–5.
26. Oliveros JC, Venny. An interactive tool for comparing lists with Venn's diagrams. 2007. Available from: <http://bioinfogp.cnb.csic.es/tools/venny/>.
27. Huang DW, Sherman BT, Lempicki RA. Systematic and integrative analysis of large gene lists using DAVID bioinformatics resources. *Nat Protoc* 2009;4:44–57.
28. Huang DW, Sherman BT, Lempicki RA. Bioinformatics enrichment tools: paths toward the comprehensive functional analysis of large gene lists. *Nucleic Acids Res* 2009;37:1–13.
29. Smith ER, Yeasky T, Wei JQ, Miki RA, Cai KQ, Smedberg JL, et al. White spotting variant mouse as an experimental model for ovarian aging and menopausal biology. *Menopause* 2012;19:588–96.
30. Lavolette LA, Ethier J-F, Senterman MK, Devine PJ, Vanderhyden BC. Induction of a menopausal state alters the growth and histology of ovarian tumors in a mouse model of ovarian cancer. *Menopause* 2011;18:549–57.
31. Wang D, DuBois RN. Immunosuppression associated with chronic inflammation in the tumor microenvironment. *Carcinogenesis* 2015;36:1085–93.
32. Hou Z, Ye Q, Qiu M, Hao Y, Han J, Zeng H. Increased activated regulatory T cells proportion correlate with the severity of idiopathic pulmonary fibrosis. *Respir Res* 2017;18:170.
33. Lee SB, Kalluri R. Mechanistic connection between inflammation and fibrosis. *Kidney Int Suppl* 2010;119:S22–6.
34. Sato N, Takasaka N, Yoshida M, Tsubouchi K, Minagawa S, Araya J, et al. Metformin attenuates lung fibrosis development via NOX4 suppression. *Respir Res* 2016;17:107.
35. St. Onge EL, Miller S, Clements E. Sitagliptin/metformin (Janumet) as combination therapy in the treatment of type-2 diabetes mellitus. *P T* 2012;37:699–708.
36. Sharma M, Beckley N, Nazareth I, Petersen I. Effectiveness of sitagliptin compared to sulfonylureas for type 2 diabetes mellitus inadequately controlled on metformin: a systematic review and meta-analysis. *BMJ Open* 2017;7:e017260.
37. Harper EI, Sheedy EF, Stack MS. With great age comes great metastatic ability: ovarian cancer and the appeal of the aging peritoneal microenvironment. *Cancers* 2018;10:pii:E230.
38. Ricard-Blum S, Baffet G, Th  ret N. Molecular and tissue alterations of collagens in fibrosis. *Matrix Biol* 2018;68–69:122–49.
39. Strupler M, Pena A-M, Hernest M, Tharaux P-L, Martin J-L, Beaurepaire E, et al. Second harmonic imaging and scoring of collagen in fibrotic tissues. *Opt Express* 2007;15:4054–65.
40. Keikhosravi A, Bredfeldt JS, Sagar AK, Eliceiri KW. Second-harmonic generation imaging of cancer. *Methods Cell Biol* 2014;123:531–46.
41. Huttunen MJ, Hassan A, McCloskey CW, Fasih S, Upham J, Vanderhyden BC, et al. Automated classification of multiphoton microscopy images of ovarian tissue using deep learning. *J Biomed Opt* 2018;23:1–7.
42. Rinkevich Y, Walmsley GG, Hu MS, Maan ZN, Newman AM, Drukker M, et al. Skin fibrosis. Identification and isolation of a dermal lineage with intrinsic fibrogenic potential. *Science* 2015;348:aaa2151.
43. Demuth H-U, McIntosh CHS, Pederson RA. Type 2 diabetes-therapy with dipeptidyl peptidase IV inhibitors. *Biochim Biophys Acta* 2005;1751:33–44.
44. Matkar PN, Singh KK, Rudenko D, Kim YJ, Kuliszewski MA, Prud'homme GJ, et al. Novel regulatory role of neuropilin-1 in endothelial-to-mesenchymal transition and fibrosis in pancreatic ductal adenocarcinoma. *Oncotarget* 2016;7:69489–506.
45. Tang Z, Lu B, Hatch E, Sacks SH, Sheerin NS. C3a mediates epithelial-to-mesenchymal transition in proteinuric nephropathy. *J Am Soc Nephrol* 2009;20:593–603.
46. Danobeitia JS, Djarnali A, Fernandez LA. The role of complement in the pathogenesis of renal ischemia-reperfusion injury and fibrosis. *Fibrogenesis Tissue Repair* 2014;7:16.
47. Fisher AJ, Cipolla E, Varre A, Gu H, Mickler EA, Vittal R. Potential mechanisms underlying tgf-  -mediated complement activation in lung fibrosis. *Cell Mol Med* 2017;3:pii-14.
48. Boire A, Zou Y, Shieh J, Macalinao DG, Pentsova E, Massagu   J. Complement component 3 adapts the cerebrospinal fluid for leptomeningeal metastasis. *Cell* 2017;168:1101–13.
49. Lech M, Anders H-J. Macrophages and fibrosis: How resident and infiltrating mononuclear phagocytes orchestrate all phases of tissue injury and repair. *Biochim Biophys Acta* 2013;1832:989–97.
50. Quatromoni JG, Eruslanov E. Tumor-associated macrophages: function, phenotype, and link to prognosis in human lung cancer. *Am J Transl Res* 2012;4:376–89.
51. Sousa S, M  att   J. The role of tumour-associated macrophages in bone metastasis. *J Bone Oncol* 2016;5:135–8.
52. Braga TT, Agudelo JSH, Camara NOS. Macrophages during the fibrotic process: M2 as friend and foe. *Front Immunol* 2015;6:602.
53. Provenzano PP, Inman DR, Eliceiri KW, Knittel JG, Yan L, Rueden CT, et al. Collagen density promotes mammary tumor initiation and progression. *BMC Med* 2008;6:11.
54. Weiskirchen R, Weiskirchen S, Tacke F. Organ and tissue fibrosis: molecular signals, cellular mechanisms and translational implications. *Mol Aspects Med* 2018;65:2–15.
55. Loughran EA, Leonard AK, Hilliard TS, Phan RC, Yemc MG, Harper E, et al. Aging increases susceptibility to ovarian cancer metastasis in murine allograft models and alters immune composition of peritoneal adipose tissue. *Neoplasia* 2018;20:621–31.
56. Vanderhyden BC. Loss of ovarian function and the risk of ovarian cancer. *Cell Tissue Res* 2005;322:117–24.
57. Bodmer M, Becker C, Meier C, Jick SS, Meier CR. Use of metformin and the risk of ovarian cancer: a case-control analysis. *Gynecol Oncol* 2011;123:200–4.
58. Urpilainen E, Marttila M, Hautakoski A, Arffman M, Sund R, Ilanne-Parikka P, et al. The role of metformin and statins in the incidence of epithelial ovarian cancer in type 2 diabetes: a cohort and nested case-control study. *BJOG* 2018;125:1001–8.
59. Wen Q, Zhao Z, Wen J, Zhou J, Wu J, Lei S, et al. The association between metformin therapy and risk of gynecological cancer in patients: two meta-analyses. *Eur J Obstet Gynecol Reprod Biol* 2019;237:33–41.
60. Kraakman MJ, Murphy AJ, Jandeleit-Dahm K, Kammoun HL. Macrophage polarization in obesity and type 2 diabetes: weighing down our understanding of macrophage function? *Front Immunol* 2014;5:470.
61. Mantovani A, Sozzani S, Locati M, Allavena P, Sica A. Macrophage polarization: tumor-associated macrophages as a paradigm for polarized M2 mononuclear phagocytes. *Trends Immunol* 2002;23:549–55.
62. Khan MA, Assiri AM, Broering DC. Complement and macrophage crosstalk during process of angiogenesis in tumor progression. *J Biomed Sci* 2015;22:58.
63. Ueha S, Shand FHW, Matsushima K. Cellular and molecular mechanisms of chronic inflammation-associated organ fibrosis. *Front Immunol* 2012;3:71.